Gait & Posture 68 (2019) 403–408

Contents lists available at ScienceDirect

Gait & Posture

journal homepage: www.elsevier.com/locate/gaitpost

Full length article

A convolutional neural network Cascade for plantar pressure images registration

Yi Xia[1], Yanlin Li[1], Lina Xun, Qing Yan, Dexiang Zhang*

Department of Electrical Engineering and Automation, Anhui University, Hefei 230601, China

ARTICLE INFO

Keywords:
Convolutional neural network
Plantar pressure image registration
Regression model

ABSTRACT

Background: Plantar pressure image (PPI) recorded in high spatial and temporal resolution is very useful in clinical gait analysis. For functional analysis of PPI, image registration is often performed to maximally correlate source image with a template image. Previous methods estimate the registration parameters by iteratively optimizing different objective functions. These methods are often computational expensive to achieve satisfactory registration accuracy.

Research question: Can we develop a single PPI registration technique that performs more rapidly than previous methods, and that also maintains adequate PPI correspondence as defined by various (dis)similarity metrics?

Methods: A cascaded convolutional neural network (CNN) was proposed for the registration of PPIs. Our model was trained to learn a regression from the difference between the template and misaligned images to the registration parameters. The registration performance was evaluated by three different metrics, i.e. the mean squared error (MSE), the exclusive or (XOR), and the mutual information (MI). For comparison, four previous methods were also implemented. These included the principal axes (PA) method, the center of pressure trajectory (COP) method, the MSE method, and the XOR method.

Results: Experimental results on a dataset with 71 PPI template-source pairs showed that the proposed CNN-based method could obtain comparable registration accuracy to the MSE and XOR method. With regards to the registration speed, registration durations (mean ± sd in seconds) per image pair were: MSE (30.584 ± 2.171), XOR (24.245 ± 1.596), PA (0.016 ± 0.003), COP (25.614 ± 0.341), and the proposed model (0.054 ± 0.007).

Significance: Our findings indicate that the proposed registration approach can achieve high accuracy but less computational time. Thus, it is more practical to utilize our pre-trained CNN-based model to develop near-real time applications for plantar pressure images registration.

1. Introduction

Plantar pressure distributions, i.e. pressure fields that act between the plantar surface of the foot and a contacted surface, are widely measured in a number of diverse fields such as sports biomechanics, clinical diagnosis as well as biomechanical analysis of gait and posture. For instance, it is helpful in the diagnosis of diabetic foot ulcers and diabetic peripheral neuropathy, which can give rise to changes in foot structure, making the foot function being affected, eventually leading to altered plantar pressure distribution [1]. In the study presented by Hahn et al. [2], plantar pressure distribution is used in the post-surgery biomechanical assessment. By analyzing the parameters of foot contact time, maximum pressure as well as contact area between women and men when they are in normal training and competition, Queen et al. [3] draw the conclusion that suitable shoes should be designed for the prevention of metatarsal stress fractures due to the different loading patterns between women and men. So far, different techniques have been developed to measure plantar pressure distribution, such as force plate [4], in-shoe plantar insole [5], as well as force platform [6]. The measured plantar pressure data during certain duration is often stored in the form of a sequence of gray images. Thus, modern digital image processing techniques can be exploited to facilitate the analysis of the plantar pressure distribution.

Image registration refers to the process of transforming one image, termed as a 'source', to match a second image, termed as a 'template'. Image registration is often a necessary preprocessing step for better

* Corresponding author.
E-mail addresses: LYLAU1314@163.com (Y. Li), xunlina@126.com (L. Xun), anhuixbt@sina.com (Q. Yan), dzxyzdx@126.com (D. Zhang).
[1] These authors contributed equally to the paper as first authors.

https://doi.org/10.1016/j.gaitpost.2018.12.021
Received 7 July 2018; Received in revised form 11 December 2018; Accepted 17 December 2018

analysis that followed. Many image registration methods tailored to plantar pressure image have been developed during the past decades. Oliveira et al. [7] presented a method that was based on the matching of the contour points to register the plantar pressure. Later, they [8] utilized cross-correlation and phase correlation in the frequency domain for the registration of plantar pressure images. Four warping registration methods [9] including principal axes, four-parameter optimal scaling, eight-parameter optimal projective and locally affine nonlinear, were introduced for plantar image registration between different subjects. Recently, Oliveira et al. [10] realized the temporal alignment of the plantar pressure image sequences by using B-splines, and spatial alignment by using several geometric transformation models.

Regression is a very useful tool used by different researchers in various fields to express a relationship between input and output variables. Linear models [11] have been successfully applied in some simple tasks, but they are limited to solve the problem when the relationships between the input and output variables are very complex. Therefore, most recent studies in regression have focused on developing non-linear models, such as kernel machines [12], tree-based ensembles [13], and decomposition via Gaussian basis [14]. During the last decade, the convolution neural network (CNN) has achieved impressive success in many signal processing problems, such as image classification [15], object detection [16] and semantic segmentation [17], due to its strong modeling capabilities. The regression model based on CNN has also attracted more and more attention in the past decades. Different applications such as human age estimation [18], human pose estimation [19], and face alignment [20] have been proposed. Compared to the previous regression model, the CNN model can learn robust features from the data automatically, which leads to a much better prediction accuracy.

This study aims to present a novel cascade CNN method for the plantar pressure images registration. Comparing to previous methods that estimate the registration parameters via an iterative optimizing process to minimize a scalar-valued metric function, our approach adopts a two-stage CNN-based framework to estimate the registration parameters step by step. Similar to many other applications, the CNN is utilized in our approach to learn robust features embedded in the images for the update of registration parameters. To the best of our knowledge, the CNN-based model has not been exploited for the registration of plantar pressure images. The experimental results show that the proposed registration method can provide not only high registration accuracy, but also high registration speed due to the model is trained offline.

2. Methods

2.1. Experiment

Thirty subjects (25 males, 5 females; male average age: 20.8 ± 4.3 years, female average age: 25.6 ± 2.3 years) were recruited from Anhui University. Prior to participation, each subject gave informed consent according to the policies of the Research Ethics Committee of the Anhui University. Each subject was asked to perform a total of six trials of self-paced walking with normal speed on a pressure-sensing-mat system (Zebris FDM-S system, Germany). The sensing area was 54.2 × 33.9 cm with a physical resolution of 1.4 sensors/cm^2, and the sampling rate was 100 Hz.

2.2. Previous methods

Principal axes (PA) [21] method is a non-optimization method, which aligns the principal coordinate system of the source image to that of the template. Following the method proposed by Harrison and Hillard [22], the PA of the plantar image is calculated as the eigenvectors of the pressure-weighted covariance matrix $\mathbf{\Sigma}$:

$$\mathbf{\Sigma} = \sum_{i,j} p_{i,j}(d_{i,j} - c_{i,j})(d_{i,j} - c_{i,j})^T \quad (1)$$

$$c_{i,j} = \frac{\sum_{i,j} p_{i,j} d_{i,j}}{\sum_{i,j} p_{i,j}} \quad (2)$$

where i, j is the horizontal and vertical position in an image coordinate system, $d_{i,j}$ is the position vector (i.e. $[i\ j]$) of each sensor's centroid and $p_{i,j}$ is the pressure at that position. $c_{i,j}$ is in fact the center of pressure (COP) of the calculated plantar image. The scaling transformation for PA method is implemented based on the ratio of foot lengths for the image pairs.

The COP trajectory, mean squared error (MSE) and exclusive or (XOR) method [23] are all optimization-based methods, and they all try to align the image pairs by minimizing respective error function whose values are defined in a searching grid of the parameter space. The COP trajectory corresponding to a peak plantar image (PPI) is a vector that contains the COPs of all the instantaneous plantar images during a walking cycle.

MSE is calculated over non-zero pixels as:

$$MSE = \frac{1}{N} \sum_{i,j} (p_{i,j}^{(0)} - p_{i,j}^{(1)})^2 \quad (3)$$

where $p_{i,j}^{(0)}$ and $p_{i,j}^{(1)}$ is the pressure value at the 2-D position (i, j) for the first and second image respectively, and N is the total number of non-zero pixels in the plantar image.

XOR is defined as:

$$XOR = \frac{|I_0 \oplus I_1|}{|I_0| + |I_1|} \times 100\% \quad (4)$$

where $|I_0|$ and $|I_1|$ are binary template as well as source images, respectively, defined by the inequality: $(I > 0)$. The symbol $\oplus$ is an exclusive OR operation.

The particle swarm optimization (PSO) algorithm [24] was used to implement the optimization of the objective function defined in COP, MSE and XOR method. To speed up the global convergence, the PA method was utilized to obtain a good start point, and then the PSO algorithm could rapidly obtain the optimal solution with a population size of 200 solutions over 20 generations.

2.3. Proposed algorithm

The proposed method consists of two stages that are connected sequentially. The first stage is for estimating the initial parameters and then performing a preliminary alignment, while the second stage is for estimating the specific registration parameters using a regression model based on the cascaded CNN. Fig. 1 shows an overview of our approach for the estimation of registration parameters.

2.3.1. Initial estimation

The transformation of a plantar pressure image was represented by four parameters, i.e., t_x, t_y, t_θ and t_α, which denoted the horizontal translation, vertical translation, rotation angle, as well as scaling ratio respectively. Before feeding the plantar pressure image into a regression model, the image was first moved in both horizontal and vertical direction so that the bounding box center of the pressure points was aligned with the center of the template image. By this way, the range of t_x, t_y and t_α could be estimated within a small range. To confine the rotation angle t_θ to a small range, we first rotated the source image to align its major axis to that of the template image. The major axis was calculated as the major eigenvector of the pressure-weighted covariance matrix [25]. The small parameter space spanned by these separate ranges could guarantee a rapid regression as well as an accurate registration.

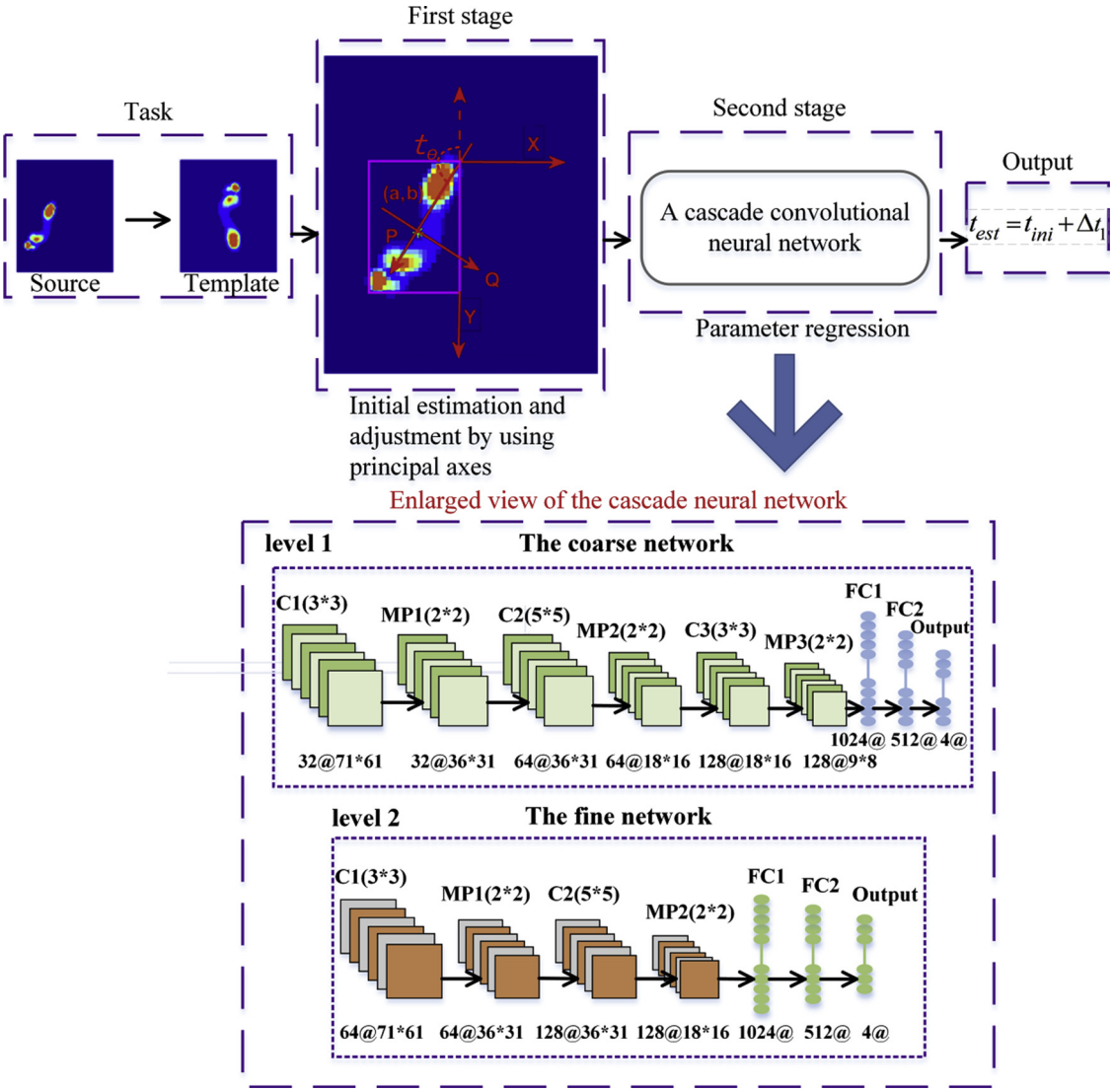

Fig. 1. An overview of the proposed method for estimation of the registration parameters. Note that "C", "MP", and "FC" are the abbreviations of "convolutional layer", "Max pooling layer", and "fully connected layer" respectively. Before "@" refers to the number of feature maps in convolutional layers or the output dimension of the fully connected layers after "@" refers to the size of feature maps. Numbers in parentheses denote the kernel parameters of the corresponding operation.

2.3.2. Cascade neural network

The regression model is a two-level cascade CNN-based neural network. It contains one coarse network and one fine network. The coarse network can provide an approximate estimation of the correct registration parameters. While the fine network plays a role that fine-tunes the registration parameters obtained at the previous level. The final estimation of the registration parameter is a combination of the outputs of the two-level networks. The architecture of two-level cascade CNN is also plotted in Fig. 1.

The coarse level network takes the source images as its input. The network at this level is made up of nine sequentially connected layers including three convolution layers, three max-pooling layers, and three fully connected layers. Supposing that $x \in R^h$ represents the plantar pressure image with h pixels, $T(x) \in R^4$ indicates the four registration parameters, the objective of the registration parameter estimation problem is to learn a non-linear mapping relationship F from the plantar pressure image space to the parameter space:

$$F: x \rightarrow T(x) \tag{5}$$

In order to get this complex nonlinear function F model, such a problem can be transformed into the minimization of an MSE function, which is defined as:

$$f = \frac{1}{g}\sum_{i=1}^{g} || y_i - F(x_i; w) ||_2^2 \tag{6}$$

where g is the amount of training samples, y_i is the label for the ith training sample, $F(x_i; w)$ is the output of the first level network for the ith training sample. The label of a training sample at this level is the ground truth of the registration parameter, that is $y_i = t_i^{gt}$.

The fine level network includes seven layers: two convolution layers, two max pooling layer, and three fully connected layers. Its task is to learn the mapping function L_k from the plantar pressure image space to the difference space of the registration parameter. The fine-tuning network minimizes the following loss function:

$$\eta = \frac{1}{g}\sum_{i=1}^{g} || \Delta y_i^{(1)} - L(x_i; w) ||_2^2 \tag{7}$$

where g is the amount of training samples, $\Delta y_i^{(1)}$ is the label, i.e., the difference between the output of the first level and the ground truth for the ith training sample. $L(x_i; w)$ is the output of the network for the ith training sample. In our study, the label for the fine-tuning level is given

by the following,

$$\Delta y_{(1)} = t_{gt} - t_{ini} \quad (8)$$

where t_{ini} is the output of the first-level network. The final output of the two-level regression network is given as

$$t_{est} = t_{ini} + \Delta t_1 \quad (9)$$

where Δt_1 is the output of the second-level network.

2.3.3. Network training

For the two-level regression network, a dataset with 100,000 images was built for its training. Our template image was selected from a male subject with an age of 24. The other images were obtained by the four transformations (i.e. scaling, horizontal or vertical shift, as well as rotation) from the template plantar pressure image. We set the horizontal translation and vertical translation parameters t_x, t_y in the range of -5 pixels to 5 pixels ($' - '$ denote the image performs translation left or down), the scaling factor t_α from 0.5 to 2, and t_θ from $-5°$ to $5°$ ($' - '$ indicates a clockwise rotation). Finally, each source image was cropped into an image with a size of 71×61 pixels as the input of cascaded CNN. In our experiments, 90% samples of our dataset were randomly chosen as training data while the rest was used as validation data. The training for the two different level of network was performed sequentially. The coarse network was trained by minimizing the objective in Eq. (6). After that, the fine network could be trained according to the objective in Eq. (7).

2.4. Performance evaluation

The registration accuracy was evaluated with the following three metrics: MSE, XOR and mutual information (MI) [26]. Additionally, the differences between the mean MSE, XOR, and MI values obtained by different registration methods were assessed using one-way MANOVA and Bonferroni post-hoc comparisons. The SPSS software (Version 19.0, SPSS Inc., Chicago, IL, USA) was adopted for all statistical analysis.

The training of our model was performed on a computer equipped with NVIDIA Tesla V100 graphics processing unit (GPU) card, CUDA Cores 5120 and 64 GB memory, while the testing of our model together with other registration methods was implemented on a computer equipped with an Intel Core i5 7500 Central Processing Unit (CPU) and 16 GB memory.

3. Results

The results of registration accuracy for different methods were shown in Table 1, and the p values from Bonferroni post-hoc tests were shown in Table 2. First of all, one-way MANOVA on the three accuracy metrics (MSE, XOR, and MI) confirmed the existence of a METHOD effect ($p < 0.001$). Then, the following observations could be made from Tables 1 and 2. The two global optimization-based methods (MSE, XOR) and our approach could provide apparently higher accuracies than the two reduction methods (PA, COP) ($p < 0.001$). For all three accuracy metrics, the COP method performed the worst among all methods ($p < 0.001$ for all the metrics). For the MSE metric, the p value for our approach and the XOR method was 0.310, while for the XOR metric, the p value for our approach and the MSE method was 1.000. Finally, for the MI metric, the above three methods had no significant difference ($p > 0.066$).

Table 2
The p-values from Bonferroni post-hoc comparisons between five registration methods (MSE, XOR, COP, PA, and Ours) on three performance metrics (MSE, XOR, and MI).

		COP	MSE[a]	XOR	PA	Ours
MSE[b]	**COP**	×				
	MSE	0.000	×			
	XOR	0.000	1.000	×		
	PA	0.000	0.000	0.000	×	
	Ours	0.000	0.008	0.310	0.000	×
XOR	COP	×				
	MSE	0.000	×			
	XOR	0.000	0.869	×		
	PA	0.000	0.000	0.000	×	
	Ours	0.000	1.000	0.011	0.000	×
MI	COP	×				
	MSE	0.000	×			
	XOR	0.000	1.000	×		
	PA	0.000	0.000	0.000	×	
	Ours	0.000	0.066	0.251	0.000	×

[a] MSE, XOR, COP, and PA represent the registration methods (see Section 2.2).
[b] MSE, XOR, and MI represent performance metrics (see Section 2.4).

The visual comparison of the registration quality for different methods was shown in Fig. 2. After registration, the image pairs registered by COP and PA method had apparent non-aligned parts. In contrast, the other three methods (XOR, MSE and our approach) could provide much better registration quality, and there was no noticeable visual difference between these three methods.

The registration speeds for different methods were also listed in Table 1. One could find from Table 1 that the registration speed of our model was significantly faster than the three optimization-based methods, i.e., the MSE, XOR and COP method, though the offline training of our network took about 2 h. The PA method owned the fastest speed due to its simpleness.

4. Discussion

In general, the more the training samples, the more robust regression model that a CNN can learn. As we know, the number of training samples that are required is determined by the size of the parameter space. The parameter space spanned by the four registration parameters is very huge, thus it is computationally prohibitive to include too many images for a robust training of the regression model. To overcome this problem, we first adopt a preliminary alignment strategy to confine the parameter space to a small range. Then 100,000 points are randomly sampled from the small 4-D parameter space. After that, our training images can be generated based on these ground truth transformation parameters.

Our experimental results show that the global optimization-based methods (MSE and XOR method) have a better registration accuracy than the reduction methods (PA and COP method), and the COP

Table 1
The performance comparison for different registration methods. All measures are expressed as its mean ± standard (SD).

Performance Measure	Registration Method					
	Pre-Reg	MSE	XOR	COP	PA	Ours
MSE(Ncm^{-2})^2	19.24 ± 5.87	1.96 ± 0.73	2.43 ± 0.89	17.45 ± 4.05	6.77 ± 2.65	3.27 ± 1.33
XOR (%)	74.84 ± 25.99	7.59 ± 2.63	5.06 ± 1.46	56.17 ± 13.99	19.63 ± 5.61	9.90 ± 3.38
MI	1.14 ± 0.28	2.43 ± 0.30	2.41 ± 0.24	1.18 ± 0.23	1.91 ± 0.23	2.31 ± 0.22
Running Times (s)		30.584 ± 2.171	24.245 ± 1.596	25.614 ± 0.341	0.016 ± 0.003	0.054 ± 0.007

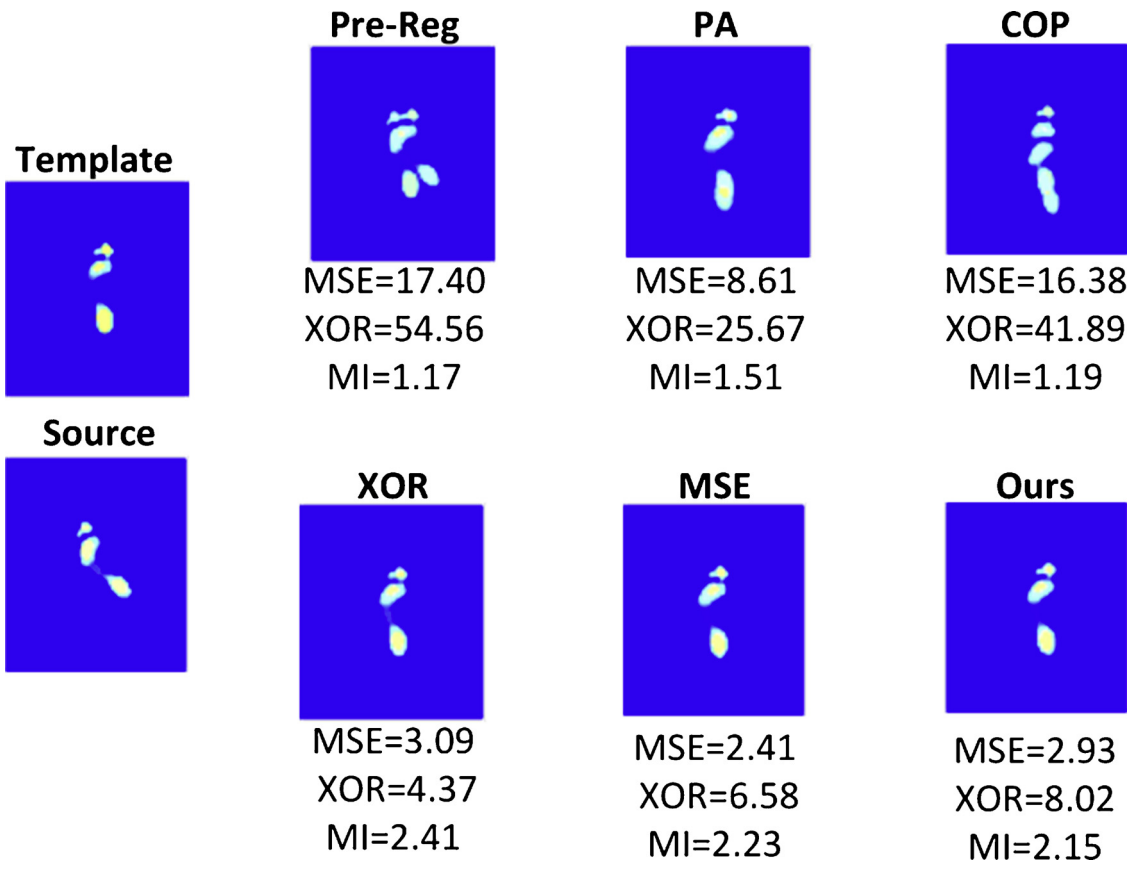

Fig. 2. Example registration. The Pre-Reg illustrates the overlapped template and source images prior to registration, the remainder of the image pairs illustrate the results of five registration methods: principal axes (PA), center of pressure trajectory (COP), exclusive OR (XOR), mean squared error (MSE), and our CNN-based method, respectively. Below each image pair, values of the (dis)similarity metrics are listed. Among these metrics, mutual information (MI) is a similarity metric, while the MSE and XOR are both dissimilarity metrics. Therefore, larger MI values imply better image correspondence, and the smallest MSE and XOR values tend to be associated with the largest MI values.

method performs the worst with regards to the accuracy. These results are consistent with that reported in a previous study [23]. Though the MSE and XOR method can provide more accurate registration, their registration speeds are obviously the slower ones compared to other methods. As a comparison, our method can provide competitive registration accuracy and near-real time speed. We attribute the high registration accuracy to the powerful modeling capability of CNN by way of different convolutional operations and nonlinear mapping operations. Furthermore, our approach adopts a cascade framework where a coarse level network is followed by a fine level network. This kind of network structure is also very important for our approach to obtain very high registration accuracy. In fact, in our experiments, we also tested a registration framework without a fine level network. The accuracy (mean ± SD) is 3.16 ± 1.81 for the MSE measure, 9.62 ± 2.31 for the XOR measure, and 2.17 ± 0.38 for the MI measure. Such a result is not as accurate as that obtained after a fine-level network. As for the registration speed, the forward propagation of the proposed model is very fast due to the moderate network depth and a limited number of the convolution kernels.

The plantar pressure image registration can provide valuable information for clinical diagnosis. Our method can predict the registration parameters quickly and accurately, which is very beneficial to clinical diagnosis. Furthermore, the proposed regression method can also be extended to other gait analysis. For example, by measuring the ground reaction force at some characteristic positions during walking and then extracting discriminative spatial or temporal features, many classification schemes [27–29] have been proposed for differentiating abnormal gaits caused by neurodegenerative diseases like Parkinson, ALS, and Huntington etc. The extension of our CNN-based regression model to such a classification task is straightforward by setting the inputs to be the PPIs and the outputs to be the corresponding class labels.

However, there are still certain limitations of the proposed method. For instance, the loss function used in our method only contains the difference between the real label and the prediction label (the parameters of image registration), we did not consider the innate relationship of the four registration parameters. As a result, the registration performance of the test images has a strong dependence on the parameter space of the training samples. Namely, if the real registration parameters of the test image are not included in the parameter space of the training images, the registration performance is not satisfactory. In the future, we plan to study how to introduce the recursion capability into the regression model to simulate the memory function of human brain, so that the model can recall the input data to further improve the prediction accuracy.

5. Conclusion

In this study, we present a novel image registration approach for plantar pressure image, which is based on a cascade CNN framework. We show that the problem of image registration can be efficiently solved by training CNN regressors to reveal the mapping from image space to the parameter space. Our experimental results demonstrate that the proposed method can provide competitive registration accuracy as well as a near-real time registration speed.

Conflict of interest

The authors declared that they have no conflicts of interest to this work.

We declare that we have no financial and personal relationships with other people or organizations that can inappropriately influence our work, there is no professional or other personal interest of any nature or kind in any product, service and/or company that could be construed as influencing the position presented in, or the review of, the manuscript entitled, “A Convolutional Neural Network Cascade for Plantar Pressure Images Registration”

Acknowledgments

This work is supported by Anhui Provincial Natural Science Foundation (grant number 1608085MF136); China Postdoctoral Science Foundation (2015M582826); National Natural Science Foundation of China (NSFC) for Youth (grant number 61602002).

References

[1] C.M. Van Schie, A review of the biomechanics of the diabetic foot, Int. J. Low. Extrem. Wounds 4 (3) (2005) 160–170.
[2] F. Hahn, C. Maiwald, T. Horstmann, P. Vienne, Changes in plantar pressure distribution after Achilles tendon augmentation with flexor hallucis longus transfer, Clin. Biomech. 23 (1) (2008) 109–116.
[3] R.M. Queen, A.N. Abbey, J.I. Wiegerinck, J.C. Yoder, J.A. Nunley, Effect of shoe type on plantar pressure: a gender comparison, Gait Posture 31 (1) (2010) 18–22.
[4] A. Karlsson, G. Frykberg, Correlations between force plate measures for assessment of balance, Clin. Biomech. 15 (5) (2000) 365–369.
[5] L. Shu, T. Hua, Y. Wang, L.Q. Qiao, D.D. Feng, X. Tao, In-shoe plantar pressure measurement and analysis system based on fabric pressure sensing array, IEEE Trans. Inf. Technol. Biomed. 14 (3) (2010) 767–775.
[6] A.M. Piazza, E.E. Binversie, L.A. Baker, B. Nemke, S.J. Sample, P. Muir, Variance associated with walking velocity during force platform gait analysis of a heterogeneous sample of clinically normal dogs, Am. J. Vet. Res. 78 (4) (2017) 500.
[7] F.P. Oliveira, J.M. Tavares, T.C. Pataky, Rapid pedobarographic image registration based on contour curvature and optimization, J. Biomech. 42 (15) (2009) 2620–2623.
[8] F.P. Oliveira, T.C. Pataky, J.M. Tavares, Registration of pedobarographic image data in the frequency domain, Comput. Methods Biomech. Biomed. Eng. 13 (6) (2010) 731–740.
[9] T.C. Pataky, N.L. Keijsers, J.Y. Goulermas, R.H. Crompton, Nonlinear spatial warping for between-subjects pedobarographic image registration, Gait Posture 29 (3) (2009) 477–482.
[10] F.P. Oliveira, J.M. Tavares, Enhanced spatio-temporal alignment of plantar pressure image sequences using B-splines, Med. Biol. Eng. Comput. 51 (3) (2013) 267–276.
[11] K. Liang, S.L. Zeger, Longitudinal data analysis using generalized linear models, Biometrika 73 (1) (1986) 13–22.
[12] M.E. Tipping, Sparse bayesian learning and the relevance vector machine, J. Mach. Learn. Res. 1 (3) (2001) 211–244.
[13] J.H. Friedman, Greedy function approximation: a gradient boosting machine, Ann. Stat. 29 (5) (2001) 1189–1232.
[14] S. Tateishi, H. Matsui, S. Konishi, Nonlinear regression modeling via the lasso-type regularization, J. Stat. Plan. Inference 140 (5) (2010) 1125–1134.
[15] A. Krizhevsky, I. Sutskever, G.E. Hinton, ImageNet classification with deep convolutional neural networks, International Conference on Neural Information Processing Systems, (2012), pp. 1097–1105.
[16] S. Ren, K. He, R. Girshick, J. Sun, Faster R-CNN: towards real-time object detection with region proposal networks, IEEE Trans. Pattern Anal. Mach. Intell. 39 (6) (2017) 1137.
[17] J. Long, E. Shelhamer, T. Darrell, Fully convolutional networks for semantic segmentation, IEEE Conference on Computer Vision and Pattern Recognition, (2015), pp. 3431–3440.
[18] X. Liu, S. Li, M. Kan, J. Zhang, S. Wu, W. Liu, et al., ageNet: deeply learned regressor and classifier for robust apparent age estimation, IEEE International Conference on Computer Vision Workshop, (2015), pp. 258–266.
[19] X. Chu, W. Ouyang, H. Li, X. Wang, Structured feature learning for pose estimation, Comput. Vision Pattern Recognit. (2016) 4715–4723.
[20] Q. Liu, J. Deng, J. Yang, G. Liu, D. Tao, Adaptive cascade regression model for robust face alignment, IEEE Trans. Image Process. 26 (2) (2017) 797–807.
[21] A. Harrison, P. Hillard, A moment-based technique for the automatic spatial alignment of plantar pressure data, Proceedings of the Institution of Mechanical Engineers, Part H: Journal of Engineering in Medicine 214 (3) (2000) 257.
[22] A.J. Harrison, P.J. Hillard, A moment-based technique for the automatic spatial alignment of plantar pressure data, Proc. Inst. Mech. Eng. H 214 (3) (2000) 257–264.
[23] T.C. Pataky, J.Y. Goulermas, R.H. Crompton, A comparison of seven methods of within-subjects rigid-body pedobarographic image registration, J. Biomech. 41 (14) (2008) 3085–3089.
[24] K.E. Parsopoulos, M.N. Vrahatis, Recent approaches to global optimization problems through Particle Swarm Optimization, Nat. Comput. 1 (2-3) (2002) 235–306.
[25] A.J. Harrison, P.J. Hillard, A moment-based technique for the automatic spatial alignment of plantar pressure data, Proceedings of the Institution of Mechanical Engineers Part H Journal of Engineering in Medicine 214 (3) (2000) 257–264.
[26] J.P.W. Pluim, J.B.A. Maintz, M.A. Viergever, Mutual-information-based registration of medical images: a survey, IEEE Trans. Med. Imaging 22 (8) (2003) 986–1004.
[27] M.R. Daliri, Chi-square distance kernel of the gaits for the diagnosis of Parkinson’s disease, Biomed. Signal Process. Control 8 (1) (2013) 66–70.
[28] M.R. Daliri, Automatic diagnosis of neuro-degenerative diseases using gait dynamics, Measurement 45 (7) (2012) 1729–1734.
[29] R. Peng, E. Karahan, C. Chao, R. Luo, Y. Geng, J.F.B. Bayard, et al., Gait influence diagrams in parkinson’s disease, IEEE Trans. Neural Syst. Rehabil. Eng. 25 (8) (2017) 1257–1267.